Available online at www.sciencedirect.com
SCIENCE DIRECT®
Journal of Nuclear Materials 350 (2006) 221–231
journal of nuclear materials
www.elsevier.com/locate/jnucmat

Spectroscopic and microscopic study of the corrosion of iron–silicon steel by lead–bismuth eutectic (LBE) at elevated temperatures

Allen L. Johnson [a,*], Eric P. Loewen [b], Thao T. Ho [a], Dan Koury [c], Brian Hosterman [c], Umar Younas [c], Jenny Welch [c], John W. Farley [c]

[a] *Department of Chemistry, University of Nevada, Las Vegas, 4505 S. Maryland Parkway, P.O. Box 4003, Las Vegas, NV 89154-4003, USA*
[b] *Idaho National Laboratory, P.O. Box 1625, Idaho Falls, ID 83415-3860, USA*
[c] *Department of Physics, University of Nevada, Las Vegas, 4505 S. Maryland Parkway, P.O. Box 4002, Las Vegas, NV 89154-4002, USA*

Received 11 October 2005; accepted 29 December 2005

Abstract

The performance of iron–silica alloys with different silicon composition was evaluated after exposure to an isothermal bath of lead–bismuth eutectic (LBE). Four alloys were evaluated: pure iron, Fe–1.24%Si, Fe–2.55%Si and Fe–3.82%Si. The samples were exposed to LBE in a dynamic corrosion cell for periods from 700 to 1000 h at a temperature of 550 °C. After exposure, the thickness and composition of the oxide layer were examined using optical microscopy, scanning electron microscopy (SEM) and X-ray photoelectron spectrometry (XPS), including sputter depth profiling. Particular attention was paid to the role, spatial distribution, and chemical speciation of silicon. Low-binding-energy silicon (probably silicates or SiO_4^{4-}) was found in the oxide; while elemental silicon (Si) was found in the metal as expected, and silica (SiO_2) was found at the bottom of the oxide layer, consistent with the formation of a layer between the oxide and the metal. Alloys with low concentrations of Si contained only silicate in the oxide. Alloys with higher concentrations of Si contained a layer of silica at the boundary between the oxide and the bulk metal. All of the alloys examined showed signs of oxide failure. This study has implications for the role of silicon in the stability of the oxide layer in the corrosion of steel by LBE.

1. Introduction

The corrosion of steel by liquid lead or by lead–bismuth eutectic (LBE) is important in two applications: in the design of fast reactors cooled by liquid lead or by LBE and in proposed schemes for transmutation of radioactive waste. In transmutation

* Corresponding author. Tel.: +1 702 895 0881; fax: +1 702 895 4072.
E-mail address: aljohnson@ccmail.nevada.edu (A.L. Johnson).

0022-3115/$ - see front matter © 2006 Elsevier B.V. All rights reserved.
doi:10.1016/j.jnucmat.2005.12.007

schemes, LBE has been proposed for use as both a coolant and as spallation target. Transmutation holds the promise of reducing the volume, half-life, and toxicity of nuclear waste. Unfortunately, LBE corrodes most engineering materials.

Future reactor concepts under active consideration include fast reactors cooled by either pure lead or lead alloys, often lead–bismuth eutectic (LBE). Lead alloy coolants offer a number of attractive properties: chemical inertness with air and water, low vapor pressure over the relevant temperature range, high boiling point, high atomic number, and favorable neutronics (high scattering and small absorption cross-sections). The significance of these properties for potential reactor design issues was reported by Spencer [1] and by MacDonald et al. [2]. One of the key limiting factors in the development and deployment of lead or lead–bismuth eutectic cooled reactor systems is the corrosion of cladding and structural materials. Russian and US experience has shown that operation at temperatures above 550 °C must be approached with caution [3–5].

In the 1950s, research into molten-Pb showed that corrosion of cladding and reactor structural materials in contact with molten-Pb-alloy is one of the key engineering issues for a Pb-cooled reactor. The main form of corrosion is the mass transfer of cladding and structural materials along a thermal gradient, via dissolution in the hot regions and precipitation in the cold regions [6]. Thus, liquid-Pb-alloy corrosion of structural steels depends heavily on the dissolution rate of the structural material in the liquid metal. The dissolution rates are affected by diffusion barriers, metal oxides, nitrides, other surface compounds, and impurities in both the molten-Pb-alloy and the structural materials [7].

In either application (fast reactor or transmutation), the corrosion problem in lead and lead–bismuth eutectic systems has been approached using one or more of the following techniques: (1) the use of corrosion-resistant Fe-based alloys, (2) the use of a thin oxide film as a barrier to corrosion. The growth and maintenance of such a film depends on active control of the oxygen level, and (3) the use of inhibitors [8]. The use of oxygen control to promote film formation in conjunction with alloys containing oxide formers such as Si and Cr has shown the most promise. However, the basis for this behavior is not well understood [9–12]. Ferritic–martensitic steels containing silicon exhibit increased corrosion resistance in liquid lead [13]. The increased corrosion resistance may be due to formation of a SiO_2 barrier film. Note that silicon has a lower solubility in lead and lead–bismuth alloys than iron or chromium [4,5]. Furthermore, silicon forms an oxide at a lower oxygen potential than Pb, Bi, Fe, and Cr. Due to the favorable thermodynamics enrichment of Si at the surface instead of preferential dissolution of iron and chromium is expected, thus developing a diffusion barrier, which will limit dissolution of the structural material into the LBE.

The present work was conducted in order to understand the role of silicon in the corrosion of steel by lead–bismuth eutectic. Iron silicon alloys are currently in widespread use as transformer cores. The easy magnetization and demagnetization of grain oriented iron silicon steels yield efficient energy transformation. These steels form a protective SiO_2 surface layer at normal temperatures, and the migration and chemistry of the silicon in the alloy controls the magnetic properties. These commercially available alloys are convenient sources of model alloys for the iron silicon system in larger contexts.

2. Review of previous studies of role of silicon in high-temperature corrosion of steel

Silicon is well known as a minor constituent added to steel to improve corrosion resistance. Schmidt and Strehblow [14] studied the growth of passivating oxide layers on iron/silicate samples under aqueous solution at two different pH conditions. Their observations were consistent with the formation of silicates, and they conclude that iron silicate is formed on the surface of iron samples having a few percent silicon.

The effect of silicon on the high-temperature corrosion of steels has been extensively studied. A variety of other workers have probed high-temperature corrosion under two very different conditions: gas phase corrosion and liquid metal corrosion. These conditions differ in important ways: in gas phase corrosion, the removal of structural metal primarily occurs with the metal in an oxidized state. In liquid metal corrosion, catastrophic metal removal occurs when the structural metal comes into contact with the molten metal environment and dissolves. In either case, corrosion resistance is improved by the formation of an inert barrier oxide, but the mechanism of metal removal is quite different.

Many gas phase experiments have been performed with oxygen concentrations comparable to atmospheric oxygen activities. In corrosion by LBE, the oxygen concentrations are much lower, being limited on the high side by the formation of lead oxide. The maximum oxygen activity in corrosion by LBE is that of decomposing lead oxide at the operation temperature. Some gas phase studies have been performed at low oxygen concentrations (such as preoxidation studies and complex and slightly oxidizing process atmospheres).

The final difference between gas phase and liquid metal corrosion is in the mechanism of removal of components of the oxide. In gas phase oxidation, the removal of oxide is normally mechanical and non-specific, whereas in liquid metal corrosion, components of the oxide are removed by dissolution, which occurs at different rates for different components of the oxide. This differential solubility of oxide components can lead to compositions and corrosion dynamics in liquid metal corrosion that differ significantly from conventional gas/liquid corrosion.

Despite these differences, there are some similarities between liquid metal corrosion and conventional high-temperature corrosion: for short exposure times we expect the oxide that forms in oxygen controlled LBE to resemble the oxide formed from similar oxygen partial pressures and temperatures in gas-phase corrosion. Many of the issues that arise in the present paper (the location and chemical state of silicon, and corrosion resistance of the resulting oxides) also arise in the case of conventional corrosion.

2.1. Previous studies of role of silicon in high-temperature corrosion of steel: gas-phase corrosion

Miner and Nagarajan [15] studied Fe–18Cr containing Si, pre-oxidized in air at 982 °C, and corroded in low-O_2 ($pO_2 \sim 10^{-18}$ atm), sulfur-containing gas, also at 982 °C. Small additions of silicon did not seem to significantly change corrosion rates, whereas large (~2.0 wt%) additions of Si led to the formation of Cr- and Si-rich scales next to the metal. Steel with Si additions of 1.5% and 2% experienced extensive spallation of the scale, and the silicon did not reduce the corrosion by sulfur.

Evans et al. [16] studied stainless steels Fe–20Cr–25Ni, a dispersion of TiN particles, and Si content ranging from 0.05% to 2.35%. Samples were exposed to a CO_2/2% CO atmosphere with small quantities of methane and water at 850 °C for exposure times up to 6000 h. Localized silicon oxide regions formed, but not a uniform barrier layer. Increased corrosion resistance occurred for Si content near 1%, with less corrosion resistance at higher or lower concentrations. Significant spallation was also found.

Dunning et al. [17] studied oxidation in air of stainless steel Fe–16Cr–16Ni–2Mn–1Mo, and various amounts of Al and Si, exposed at 700 °C and 800 °C for 1000 h. SEM and ESCA studies suggest that the effect of minor Si addition on oxidation resistance at 800 °C may be associated with grain-boundary networks of SiO_2.

Ishitsuka et al. [18] studied oxidation of Fe–9Cr steel by high pressure steam at temperatures ranging from 500 to 700 °C for 500 h. At 0.5% Si, the formation of a silicon-containing layer was found to be temperature-dependent between 600 °C and 700 °C. At 600 °C, the silicon was observed to be distributed uniformly in the inner oxide, whereas at 700 °C, a layer at the oxide–metal boundary was observed. Silicates (Fe_2SiO_4) were found by XRD in the oxide layer at 650 °C but not at 700 °C, where only Cr_2O_3 was observed. Amorphous SiO_2 was found in the oxide layer. They conclude that quite likely the formation of amorphous SiO_2 films accounts for the protective effect of Si at 700 °C. They speculate that the complex behavior observed near 650 °C is due to the onset of FeO formation.

Kumar and Douglass [19] examined the corrosion of Fe–14Cr–14Ni with 1% and 4% Si in air at 900 °C and 1100 °C. The addition of Si enhances the protective role of Cr: in samples with 4% Si, Cr_2O_3 was found over an inner layer containing Si oxides, while formation of iron oxides was completely suppressed.

Stott et al. [20,21] studied Fe–14Cr and Fe–28Cr at 1000 °C. A protective layer formed after several hundred hours of exposure. However, under non-isothermal conditions, spallation failure of the oxide layer occurred.

Hoelzer et al. [22] studied the air oxidation of Y_2O_3-dispersed Fe–13Cr at 700, 800, and 900 °C for 10 000 h. The Si concentration was 0.05 wt%, and at 700 °C and 800 °C the oxide was a layer of silicon oxide under the chromium oxide. In contrast to the reports summarized above, they observed continuous 0.3 μm-(700 °C) and 0.9 μm-(800 °C) thick silicon oxide layers.

Huntz et al. [23] studied Fe–9Cr with 0.5–4% Si exposed to a pure oxygen atmosphere or an

$Ar/H_2/H_2O$ atmosphere ($pO_2 \sim 10^{-18}$ atm) at 600 °C and 950 °C for 24 h. Silicon addition was found to modify the Fe/Cr oxide scales. Segregation of Si, the formation of a SiO_2 layer, and the conditions for formation of a protective Cr_2O_3 oxide layer were investigated. They found that the addition of (3% and 4%) Si resulted in a twofold reduction in the diffusion rate of Cr, compared to undoped steel. They conclude that Si is not forming an effective diffusion barrier, but instead is modifying the oxygen concentration to drive the formation of chromia.

2.2. Review of recent studies of corrosion of steel by LBE

Recent studies of the corrosion of steel by static LBE include the work of Kurata et al. [24,25], Soler et al. [26], Furukawa et al. [27], Martin et al. [28], and Gnecco et al. [29]. Studies in flowing LBE include the work by Kondo et al. [30], Zhang et al. [31], Mueller et al. [32], Aiello et al. [33], Deloffre et al. [34], Balbaud-Celerier and Terlain [35], and Ilincev et al. [36]. The most relevant recent work is that of Ilincev et al. [36], who studied some twenty varieties of steel, including Si-containing alloys. Ilincev et al. performed corrosion tests on 20 types of steels in flowing LBE at 400 °C and 500 °C using different oxygen concentrations. The impact of Fe, Cr, Ni, Mn, Si, Al and Mo content on the corrosion stability of these steels was measured, as was the effect of passivation of the surface before exposure to LBE, by creation of thin spinel or oxide surface layers. Barbier and Rusanov [37] studied corrosion of steel in flowing LBE at low oxygen concentrations ($1–2 \times 10^{-6}$ wt%), at temperatures of 300 °C and 470 °C and exposure times up to 3116 h. They found the formation of a protective oxide film of magnetite, Fe_3O_4. Three steels were studied: T91, EP823 (which contains 2% Si), and Optifer IV. The presence of silicon in the EP823 steel reduces the growth rate of the oxide.

In previous work by the present authors [38], the importance of surface preparation in the corrosion of 316 stainless steel by LBE was investigated. Two samples with the same composition but different surface preparations were studied: a cold-rolled sample was compared with an annealed sample. One of the present authors, Loewen [39] studied the corrosion of 316L and other steels in a stirred isothermal LBE bath at 823 K and 923 K for 1000 h. Oxide thicknesses of 5–33 μm were found.

3. Experimental apparatus

3.1. Materials

The Idaho National Laboratory (INL) forced-convection corrosion cell, shown in Fig. 1, consists of an externally heated vessel with a shroud and gas flow system. Flow is induced by the injection of gas at the bottom of the test section. The rising gas bubbles cause flow to proceed upward in the region inside the shroud and down in the region outside the shroud. The gas composition and flow rates, heat input, and shroud and vessel dimensions are adjusted to control LBE coolant flow rate, temperature, and oxygen potential within the vessel. Test coupons are placed on the lance, also used for gas injection, at the center of the vessel, as shown in the lower right of Fig. 1. The test coupons are separated from each other and from the lance by alumina spacers. The lance, and hence the specimens, could be removed at selected intervals for examination. The detailed modeling and measurement of the liquid flow has been reported in previous publications [40].

A resistance furnace heats the experimental apparatus, and gas injection drives circulation of LBE, causing isothermal conditions. Fig. 1 shows isothermal conditions in the presence of gas injection and a temperature gradient without gas injection. The corrosion cell for these experiments was fabricated from carbon steel, which introduces a small contamination of the LBE in the form of iron, at a lower level of contamination compared to the stainless steels or zirconium used in our previous experiments [41].

System chemistry was monitored through gas phase and post experiment liquid metal chemical analysis. A mass spectrometer and O_2 meter measured the gas composition entering and exiting the corrosion cell. The mass spectrometer can accurately measure the O_2 level down to ~10 ppm. The oxygen meter, a Thermox II® system, is a self-contained portable analyzer using an electrochemical cell made of ZrO_2 heated to 760 °C, with a lower detection limit of 0.1 ppm O_2. The O_2 potential was determined by continuously analyzing the gas stream entering and leaving the corrosion cell during the experiment, under the assumption of equilibrium between the gas and the liquid phase.

The system oxygen potential was controlled through by a carbon buffer system ($C/O_2/CO/CO_2$), which uses solid and gaseous C to control

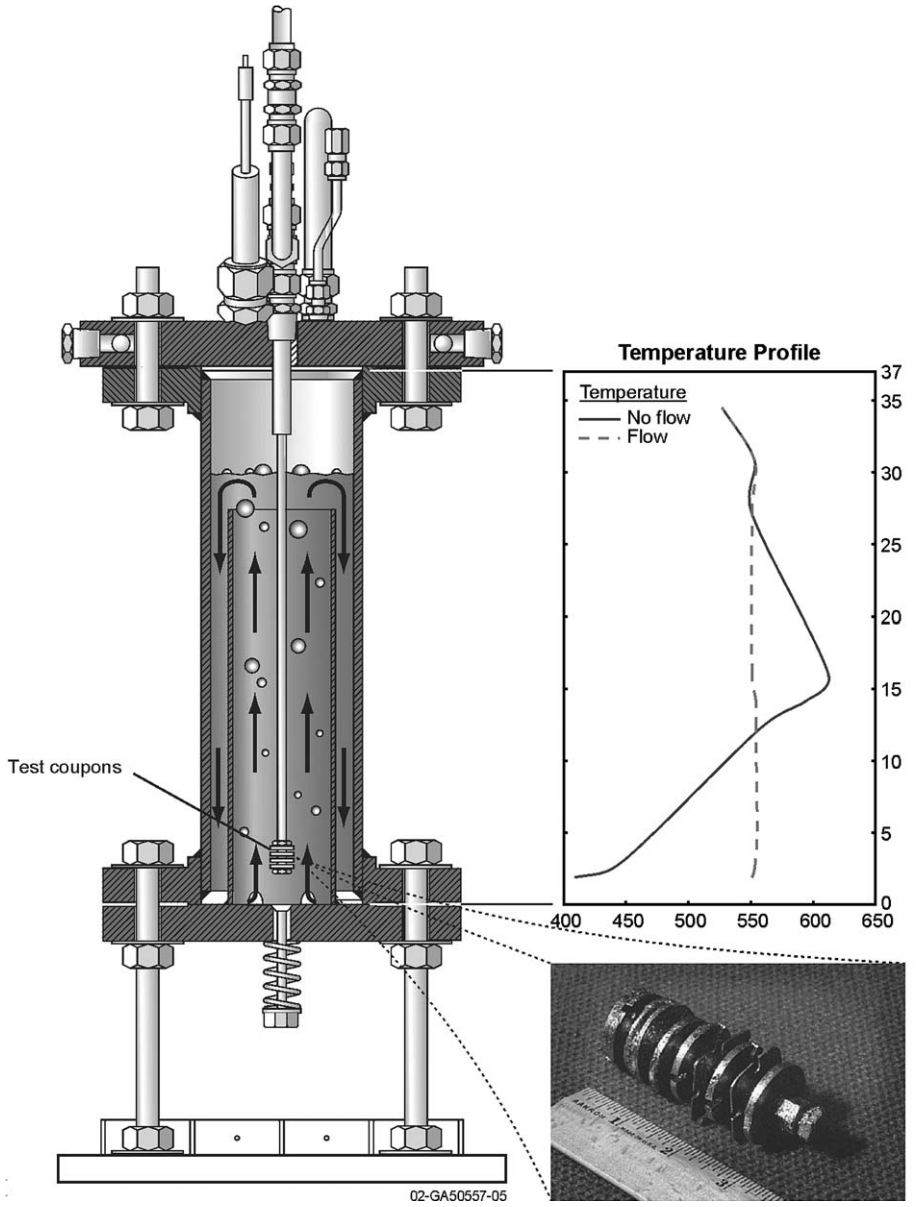

Fig. 1. Diagram of LBE test facility at INL.

the O_2 level in the LBE. The system, developed and provisionally patented at INL, provided acceptable control of the O_2 partial pressure within the range of 10^{-27}–10^{-40} atm.

3.2. Fe–Si samples before exposure

Table 1 shows the elemental composition of the Fe–Si samples before exposure to LBE. The Fe–Si alloys, obtained from commercial suppliers, have different Si contents. The four samples had Si contents of 0.05, 1.24, 2.55, and 3.82 wt%. No other elements were present in significant amounts.

3.3. Analytical equipment

Samples were removed from LBE cross-sectioned, mounted and polished to a surface roughness of 0.3 μm using the INL metrological laboratory and the facilities at UNLV.

The polished surface analysis was performed at UNLV EMIL (Electron Microscope Imaging

Table 1
Summary of material chemistries

Metal	Concentration (wt%)											
	Fe	Si	P	S	Mo	Cu	Cr	Al	Ti	C	Mn	Ni
Fe	Bal	0.05	0.007	0.016	0.017	0.03	0.04	0.031	0.002	0.02	0.31	0.03
Fe–1.24%Si	Bal	**1.24**	0.006	0.001	0.01	0.03	0.09	0.005	0.003	0.01	0.04	0.08
Fe–2.55%Si	Bal	**2.55**	0.003	0.001	0.10	0.03	0.08	0.003	0.006	0.017	0.12	0.15
Fe–3.82%Si	Bal	**3.82**	0.022	0.025	–	–	–	–	–	0.011	0.24	–

Laboratory), the UNLV XPS facilities, and the William R. Wiley Environmental Molecular Sciences Laboratory (EMSL) located on the campus of the Pacific Northwest National Laboratory in Richland, Washington.

The XPS instrument at UNLV is a Surface Science Instruments SSX-100 which has been fitted with a Nonsequitur Technologies Model 1401 ion gun for sputtering. The XPS binding analyses were references to the adventitious carbon 1s line at 284.6 eV. The X-ray source for the XPS was a monochromatized and refocussed aluminum Kα (1486 eV) source with a 0.1–1.0 mm diameter X-ray spot size. The SEM at UNLV was a JEOL JMS-5600 with an Oxford EDS detector.

At the EMSL user facility both an Auger electron spectroscopy (AES) and X-ray photoelectron spectrometer (XPS) were used for surface analysis. The AES used was Model 680 Auger electron spectroscopy/scanning Auger microprobe (SAM). The AES instrument provides information about elemental composition of the cross-sectioned surface at a beam size down to 10 nm. In the beam rastering mode secondary electron line maps across the interface were produced on most samples. This technique allowed determination of compositions of the interfaces between LBE and alloy.

The XPS used at the EMSL user facility was a Physical Electronics Instruments model Quantum 2000 X-ray photoelectron spectrometer with a focused monochromatic Al Kα X-ray beam that was varied from 10 μm in diameter to approximately 200 μm. The beam was rastered over the interface to determine chemical composition of the Si present.

4. Results

SEM investigations showed the oxide layers to be of variable thickness and to be subject to frequent failures, leading to pockets of LBE in the steel surface. Detached oxide layers have been observed next to the metal in alloys with very low or very high silicon content: Fig. 2(a) shows a layer of iron oxide in the LBE, and Fig. 2(b) shows a layer of silicon oxide buried in the surface iron oxide. A trend

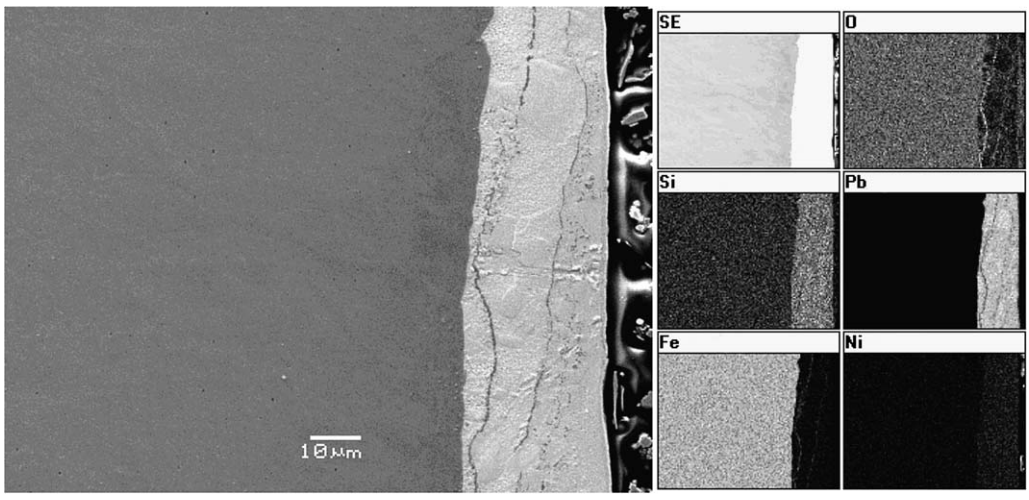

Fig. 2(a). Transverse SEM image and atoms maps of pure iron, showing a detached iron oxide layer floating in the LBE next to the surface of the iron.

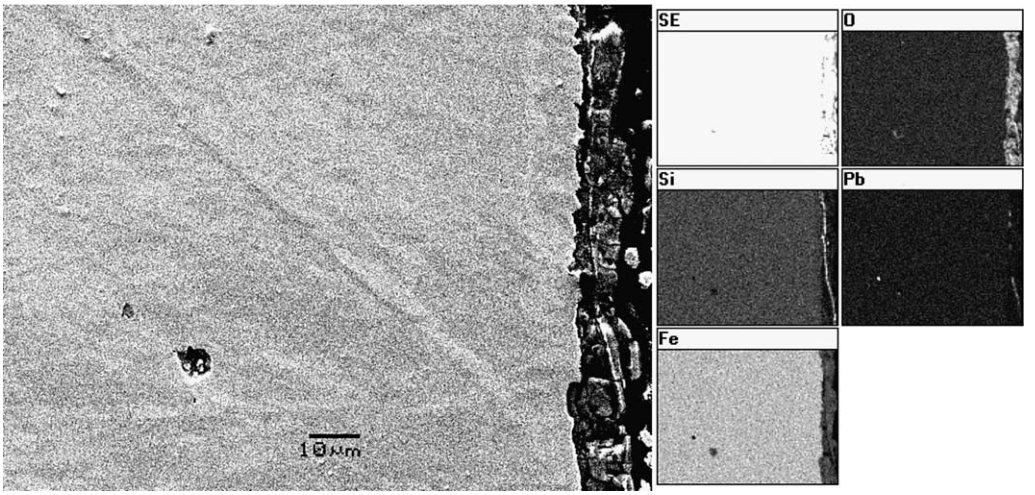

Fig. 2(b). Transverse SEM image and atoms maps of 3.82% Si in iron, showing a detached silicon oxide layer embedded in the iron oxide on the surface.

was observed in our samples: the higher silicon alloys have thicker iron oxide layers.

The XPS investigations show a thin (1.5–2 μm) oxide layer on the pure iron specimen (Fig. 3(a)). The iron/silicon alloys shows a much broader transition from oxide to underlying metal, due to a much more irregular interface/internal oxidation (Figs. 3(b), 3(c), 3(d)). Enhancement of the silicon

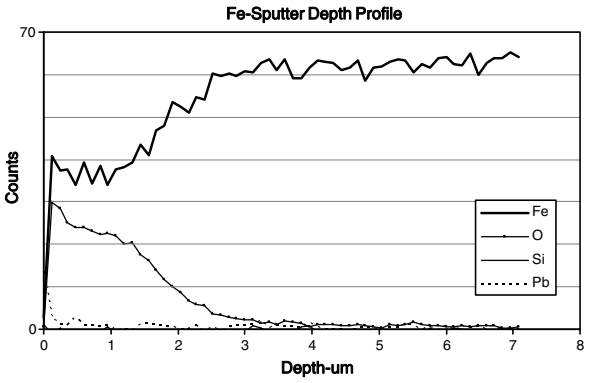

Fig. 3(a). Sputter depth profile (SDP) of nearly pure iron.

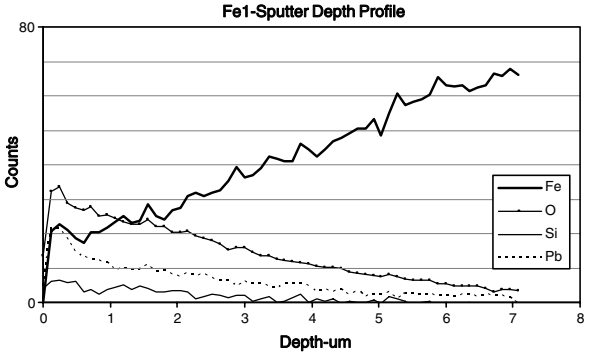

Fig. 3(b). SDP of 1.24 wt% Si alloy.

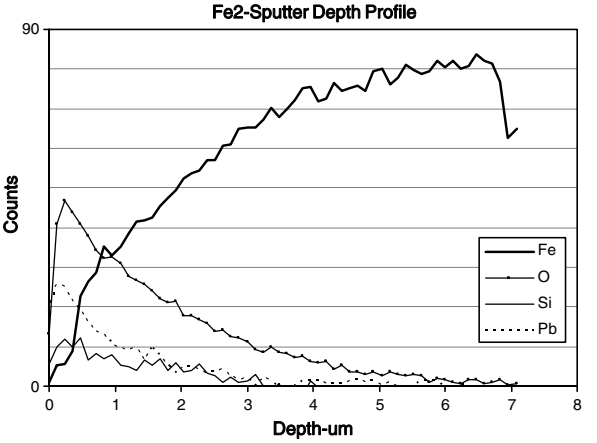

Fig. 3(c). SDP of 2.55 wt% Si alloy.

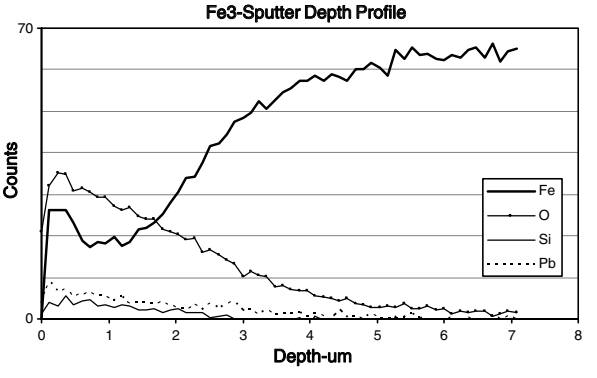

Fig. 3(d). SDP of 3.82 wt% Si alloy.

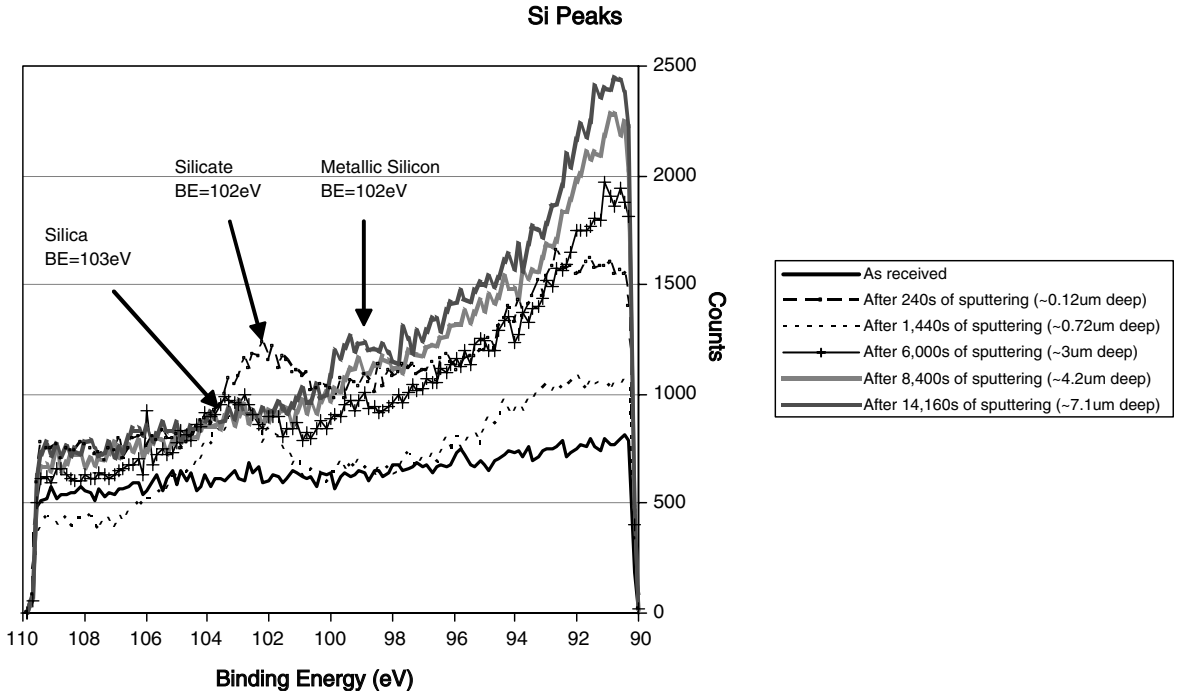

Fig. 4. Silicon species found in 3.82 wt% Si alloy as a function of sputter depth (~0.5 nm/sec sputter rate).

in the oxide was observed, and a 50% depletion of the silicon was found in the alloy layer immediately under the oxide layer. The chemical state of the silicon changes as a function of sputter depth. In the low silicon alloys, the silicon 2p line appears at a binding energy of 102 eV (SiO_3^{2-} and SiO_4^{4-}) at all depths of the oxide. In the high silicon alloy (Fig. 4), the silicon 2p peak is found at 102 eV near the LBE interface, but changes to 103 eV (SiO_2) deeper in the oxide layer. These assignments are consistent with XPS measurements reported by Seyama et al. [42].

The bottom of the sputter pit after sputter depth profiling was examined using SEM. In some instances a residual silicon oxide layer was observed at the oxide/metal interface (Fig. 5(a)), and pits in

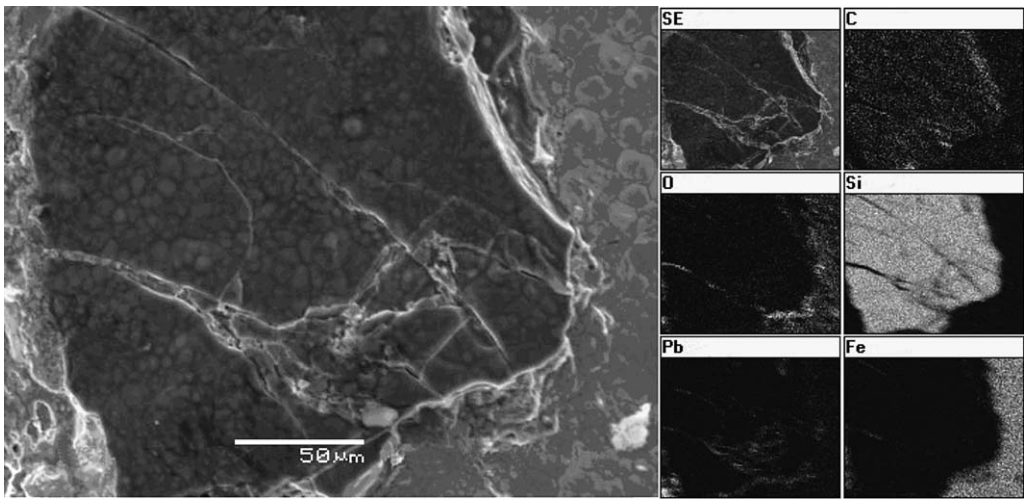

Fig. 5(a). Silicon-containing chip at the bottom of a sputter pit in 1.24 wt% silicon alloy.

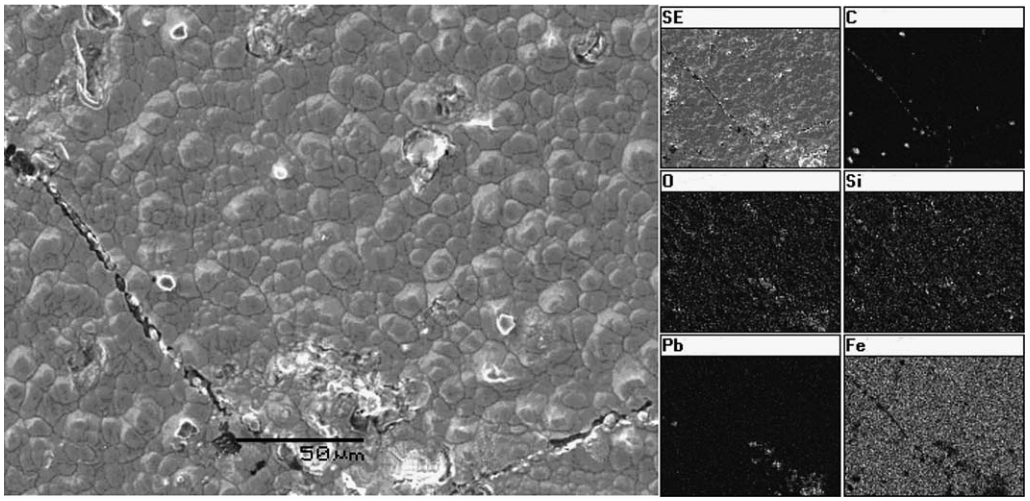

Fig. 5(b). Inclusions, LBE pit at grain boundaries at the bottom of a sputter pit in 3.82 wt% silicon alloy.

the metal filled with LBE were observed. Particle inclusions were observed at alloy grain boundaries (Fig. 5(b)), composed of varying combinations of carbon, silicon, and oxygen with the silicon/oxygen inclusions found closer to the oxide/alloy interface.

5. Discussion

The role of silicon in the corrosion of steel by oxygen controlled LBE is complex, with several competing processing controlling the final outcome. In particular the presence of silicon modifies the other oxides present in steel scales (chromia, iron oxides) as found by Huntz et al. [23] among others. Our model system studies are not expected to give the final answer, but rather to indicate the kinds of species and processes likely to occur in the final system.

In our studies silicon was found to be concentrated in the oxide layer, showing a driving force moving the silicon from the alloy to the oxide. This is consistent with the findings of other workers (e.g., Dunning et al. [17]) for most of the gas phase steel studies. In the case of the 3.82 wt% silicon alloy, the amount of silicon in the oxide was high enough to lower the ratio of iron present. In this stirred isothermal LBE exposure, significant silicon was found in the LBE that stuck to the samples after exposure. This indicates that in contrast to the gas phase studies there is significant silicon removal from the developing scales.

XPS investigations found that silicon was metallic in the alloy, as expected, and occurred in two different oxidized states in the oxide. Close to the LBE/oxide interface, silicon was found at 102 eV binding energy, and closer to the oxide/alloy interface silicon was found at 103 eV. The peak at 102 eV is characteristic of two different silicon oxides: SiO_3^{2-} and SiO_4^{4-}, silicate and e.g., olivine, respectively. These oxides of silicon can form combinations with metals and oxides which may be more stable than the starting materials. Other workers have reported Fe_2SO_4 in the scales (e.g., Schmidt and Strehblow [14], Ishitsuka et al. [18]). The present work is the first observation that the formation of silicates in the scale is dependent both on the concentration of the silicon and on the location within the scale.

The silica (SiO_2) found closer to the oxide/metal interface has been suggested as a protective diffusion barrier layer. The present study indicates that this layer is not strongly adherent, (as is commonly claimed for silicon concentrations above ~1% in the gas phase studies) and in the case of the silicon oxide layer found buried in the iron oxide layer, there was no evidence that the presence of the silicon oxide layer inhibited the formation of iron oxide in its vicinity. This is consistent with the work of Huntz et al. [23]. The discovery of silica in the near surface intergranular region suggests that oxygen and silicon are mobile enough to reach the reacting surface, even though the oxygen in particular is expected to be large with respect to the oxide lattice, and thus move via defects.

The observation of these various oxidation states of silicon suggests a new possibility. It must be

possible to change the oxidation state of the silicon in the O/LBE environment. Thus, silicon oxides may form a sink/source for oxygen in these low oxygen supply/mobility systems. This has been suggested as an explanation for the tendency of silicon-containing steels to form chromia instead of iron oxides [23].

Finally, the depletion of the silicon in the alloy underneath the oxide in all of these iron/silicon alloys suggest that in a real system, where failures of the protective oxide must be robustly repaired by in situ oxidation, the resistance of the protective layer to damage may be adversely affected by slow transport of alloying materials through the alloy to the near surface region. The gas phase studies at short times indicate that a contiguous silica layer is not formed: the high-temperature/long time experiments do see thick silica layers. If the LBE environment is disruptive to the scale by spallation or dissolution, then the desired steady state thick silica layer may not be formed.

6. Conclusions

The results of corrosion tests, conducted at INL and analyzed at UNLV and EMSL, show the effect of Si in iron. In general, the tests conducted with different concentrations for Si in iron show increasing oxide thickness with silicon concentration. Three different forms of silicon were found: silicon metal in the alloy, silicon dioxide close to the oxide–metal interface, and various silicates at the top of the oxide layer.

Our data is consistent with the formation of a silicon-oxide-containing layer between the oxide and the metal, but the layer is not necessarily protective. In our highest-silicon alloy (3.83 wt%) the iron concentration was found to decrease in the oxide layer where the silica was found. This silicon, in the form of silicon and silicates, appears to stabilize the oxide layer.

We are currently investigating iron–silicon–chromium systems, which are closer to the steels to be used in LBE facilities. In our laboratory, we are undertaking studies of high-temperature corrosion of steel in the gas phase and in LBE.

Acknowledgements

This work was supported through the INL Long-Term Research Initiative Program under DOE Idaho Operations Office Contract DE-AC07-99ID13727. A portion of the research described in this paper was performed in the Environmental Molecular Sciences Laboratory, a national scientific user facility sponsored by the Department of Energy's Office of Biological and Environmental Research located at Pacific Northwest National Laboratory. Jenny Welch was supported by the REU program of the National Science Foundation under grant PHY-0139584. A portion of this research was performed at the University of Nevada, Las Vegas under the auspices of the Transmutation Research Program of the Harry Reid Center for Environmental Studies. Support by the DOE Office of Nuclear Energy, Science and Technology, under the Advanced Fuel Cycle Initiative contracts DE-FG04-2001AL67358 and DE-AC03-76SF00098 is gratefully acknowledged.

References

[1] B.W. Spencer, The rush to heavy liquid metal reactor coolants – gimmick or reasoned, in: Proceedings of 8th International Conference of Nuclear Engineering, ICONE-8, April 2–6, Baltimore, MD, USA, 2000.
[2] P.E. MacDonald et al., Design of an actinide burning, lead or lead–bismuth cooled reactor that produces low cost electricity, INEEL/EXT-01-01376, MIT-ANP-PR-083, INEEL/MIT FY-01 Annual Report, October, 2001.
[3] B.F. Gromov, V.M. Dekusar, E. Yefimov, A.G. Kalashnikov, M.P. Leonchuk, D. Pankratov, Y.G. Pashkin, V.N. Stepanov, V.V. Chekunov, V.S. Stepanov, M.L. Kulikov, S.K. Leguenko, Lead–bismuth as a perspective coolant for advanced reactors and accelerator-based plants, in: Proceedings of the International Topical Meeting on Advanced Reactors Safety, Pittsburgh, April 1994.
[4] J.R. Weeks, A.J. Romano, Corrosion 25 (1969) 131.
[5] J.R. Weeks, Nucl. Eng. Des. 15 (1971) 363.
[6] N. Li, J. Nucl. Mater. 300 (2002) 73.
[7] W.D. Manly, Anto de S. Brasunas, Interim report on static liquid-metal corrosion, Report from ORNL Metallurgy Division, 1954.
[8] R.G. Ballinger, Y. Lim, An overview of corrosion issues for the design and operation of lead and lead–bismuth cooled reactor systems, Nucl. Technol. in press.
[9] J.R. Weeks, C.J. Klamut, Liquid metal corrosion mechanisms, in: Proceedings of the Conference on Corrosion of Reactor Materials, Europahaus, Salzburg, Austria, 4–8 June, 1962.
[10] G.Y. Lai, High Temperature Corrosion of Engineering Alloys, ASM International, 1990.
[11] G. Long, A.W. Thorley, Mechanisms of liquid-metal corrosion, in: L.L. Shrier et al. (Eds.), Corrosion, Butterworth-Heinimann, 1994.
[12] T.H. Alden, MS Thesis, MIT, 1957.
[13] D.H. Kirkwood, J. Chipman, J. Phys. Chem. 65 (1961) 1082.
[14] C. Schmidt, H.-H. Strehblow, Surf. Interf. Anal. 27 (1999) 984.
[15] R.G. Miner, V. Nagarajan, Oxid. Met. 16 (1981) 295.

[16] H.E. Evans, D.A. Hilton, R.A. Holm, S.J. Webster, Oxid. Met. 19 (1983) 1.
[17] J.S. Dunning, D.E. Alman, J.C. Rawers, Oxid. Met. 57 (2002) 409.
[18] T. Ishitsuka, Y. Inoue, H. Ogawa, Oxid. Met. 61 (2004) 125.
[19] A. Kumar, D.L. Douglass, Oxid. Met. 10 (1976) 1.
[20] F.H. Stott, G.J. Gabriel, F.I. Wei, G.C. Wood, Mater. Corros. 38 (2004) 521.
[21] F.H. Stott, G.C. Wood, J. Stringer, Oxid. Met. 44 (1995) 113.
[22] D.T. Hoelzer, B.A. Pint, I.G. Wright, J. Nucl. Mater. 283–287 (2000) 1306.
[23] A.M. Huntz, V. Bague, G. Beauple, C. Haut, C. Severac, P. Lecour, X. Longaygue, F. Ropital, Appl. Surf. Sci. 207 (2003) 255.
[24] Y. Kurata, M. Futakawa, S. Saito, J. Nucl. Mater. 343 (2005) 333.
[25] Y. Kurata, M. Futakawa, S. Saito, J. Nucl. Mater. 335 (2004) 501.
[26] L. Soler, F.J. Martin, F. Hernandez, D. Gomez-Briceno, J. Nucl. Mater. 335 (2004) 174.
[27] T. Furukawa, G. Muller, G. Schumacher, A. Weisenburger, A. Heinzel, K. Aoto, J. Nucl. Mater. 335 (2004) 189.
[28] F.J. Martin, L. Soler, F. Hernandez, D. Gomez-Briceno, J. Nucl. Mater. 335 (2004) 194.
[29] F. Gnecco, E. Ricci, C. Bottino, A. Passerone, J. Nucl. Mater. 335 (2004) 185.
[30] M. Kondo, M. Takahashi, T. Suzuki, K. Ishikawa, K. Hata, S. Qiu, H. Sekimoto, J. Nucl. Mater. 343 (2005) 349.
[31] J. Zhang, N. Li, Y. Chen, A.E. Rusanov, J. Nucl. Mater. 336 (2005) 1.
[32] G. Mueller, A. Heinzel, J. Konys, G. Schumacher, A. Weisenburger, F. Zimmermann, V. Engelko, A. Rusanov, V. Markov, J. Nucl. Mater. 335 (2004) 163.
[33] A. Aiello, M. Azzati, G. Benamati, A. Gessi, B. Long, G. Scaddozzo, J. Nucl. Mater. 335 (2004) 169.
[34] Ph. Deloffre, A. Terlain, J. Nucl. Mater. 335 (2004) 244.
[35] F. Balbaud-Celerier, A. Terlain, J. Nucl. Mater. 335 (2004) 204.
[36] G. Ilincev, D. Karnik, M. Paulovic, A. Doubkova, J. Nucl. Mater. 335 (2004) 210.
[37] F. Barbier, A. Rusanov, J. Nucl. Mater. 296 (2001) 231.
[38] A.L. Johnson, D. Parsons, J. Manzerova, D.L. Perry, D. Koury, B. Hosterman, J.W. Farley, J. Nucl. Mater. 328 (2004) 88.
[39] E.P. Loewen, H.J. Yount, K. Volk, A. Kumar, J. Nucl. Mater. 321 (2003) 269.
[40] E.P. Loewen, C.B. Davis, P.E. MacDonald, A Technique for Dynamic Corrosion Testing in Liquid Lead Alloys, ICONE-8, Baltimore, MD, April 2000, Paper-8245, 2000.
[41] E.P. Loewen, P.E. MacDonald, 2001, Heavy Metal Coolant Corrosion Testing Using a Gas Lift Apparatus, ANS Annual Winter meeting, Reno, NV, November 2001; E.P. Loewen, Philip E. MacDonald, 2001, Corrosion of Zirconium, 316, 410SS, F-22, and HT-9 Exposed to High Temperature Heavy Metal Coolant Under Extreme Conditions, American Nuclear Society Annual Winter meeting, Reno, NV, November 2001.
[42] H. Seyama, D. Wang, M. Soma, Surf. Interf. Anal. 36 (2004) 609.